ORIGINAL ARTICLE

A quartz crystal microbalance study of *β*-cyclodextrin self assembly on gold and complexation of immobilized *β*-cyclodextrin with adamantane derivatives

Kevin Hing-Nin Poon · Yu-Ling Cheng

Abstract Quartz crystal microbalance (QCM) was used to study the self-assembly of per-6-thio-*β*-cyclodextrin (t$_7$-*β*CD) on gold surfaces, and the subsequent inclusion interactions of immobilized *β*CD with adamantane-poly(ethylene glycol) (5,000 MW, AD-PEG), 1-adamantanecarboxylic acid (AD-C) and 1-adamantylamine (AD-A). From a 50 μM solution of t$_7$-*β*CD in 60:40 DMSO:H$_2$O, a t$_7$-*β*CD layer was formed on gold with surface density of 71.7 ± 2.7 pmol/cm^2, corresponding to 80 ± 3% of close-packed monolayer coverage. Gold sensors with immobilized t$_7$-*β*CD were then exposed alternately to six different concentrations of AD-PEG, 500 μM AD-C or 500 μM AD-A aqueous solutions for association, and water for dissociation. Association of AD-PEG conformed to a Langmuir isotherm, with a best fit equilibrium constant $K = 125{,}000 \pm 18{,}000$ M^{-1}. For AD-C and AD-A, association (k_a) and dissociation (k_d) rate constants were extracted from kinetic profiles by fitting to the Langmuir model, and equilibrium constants were calculated. The parameters for AD-C were found to be: $k_a = 100 \pm 5$ M^{-1} s^{-1}, $k_d = 110\ (\pm 18) \times 10^{-4}$ s^{-1}, and $K = 9{,}400 \pm 1{,}700$ M^{-1}. For AD-A, $k_a = 58 \pm 6$ M^{-1} s^{-1}, $k_d = 154\ (\pm 7) \times 10^{-4}$ s^{-1}, and $K = 3{,}800 \pm 400$ M^{-1}. The results demonstrate the utility of QCM as a tool for studying small molecule surface adsorption and guest–host interactions on surfaces. More specifically, the kinetic and thermodynamic data of AD-C, AD-A, and AD-PEG inclusion with immobilized t$_7$-*β*CD form a basis for further surface association studies of AD-X

conjugates to advance surface sensory and coupling applications.

Keywords Adamantane · Host–guest interactions · Immobilized cyclodextrin · Quartz crystal microbalance · Surface association kinetics

Introduction

Cyclodextrins (CD) are macrocyclic carbohydrate molecules that can form inclusion complexes by enclosing molecules in the internal cavity of their torus-shaped structure. The strength of complexation is dependent on van der Walls forces, steric and solvent effects, and most importantly the hydrophobic effect comprising the penetration of hydrophobic parts of the guest molecule into the CD cavity and the dehydration of the guest molecule [1, 2].

CD-guest inclusion complexes can increase the chemical stability of the guest by preventing oxidation, photodegradation and evaporation; mask odours and neutralize taste; increase water solubility and enhance mixing of otherwise incompatible compounds [3]. These properties have fueled CD use commercially, as they are widely exploited in separations technologies, food processing and pharmaceutical formulations [4]. CDs have also been exploited in immobilized form. Immobilized CD's have been used as the chromatographic stationary phase in HPLC, TLC and CE [1, 5]. Electrode coatings containing CD have been used to concentrate specific ionic species onto surfaces by inclusion complexation [6]. Several optical detection schemes have used fluorophores tethered directly to immobilized CDs to enhance fluorescence signals upon inclusion [7–11]. Yet another study has used a Tb^{3+}-CD conjugate to generate absorption-energy transfer emissions for sensor applications [12].

K. H.-N. Poon · Y.-L. Cheng (✉)
Department of Chemical Engineering and Applied Chemistry,
Institute of Biomaterials and Biomedical Engineering,
University of Toronto, Toronto, ON, Canada M5S 3E5
e-mail: ylc@chem-eng.toronto.edu

Thermodynamics of complexation between various guests and natural and derivatized CDs in solution have been extensively studied [3, 13–16]. The equilibrium constant of complexation in solution, obtained by either measuring equilibrium species concentrations, or by independently determining enthalpy and entropy of complexation, ranges from 10^2 M^{-1} to 10^4 M^{-1} for βCD complexes, and can be as high as 10^7 M^{-1} for complexes of modified βCDs such as ditopic species [17].

Adamantane, an apolar cage hydrocarbon, forms one of the strongest inclusion complexes with βCD, with equilibrium constants above 10^4 M^{-1} [2]. Complexation between βCD and adamantane or its derivatives have been exploited for gene delivery [18–20], molecular linking [21–23] and sensor applications [24–26]. Despite its uses in various applications, few data exist for the kinetic and thermodynamic properties of complexation between adamantane and βCD.

Quartz crystal microbalance (QCM) is a technique widely used to measure real-time, label-free surface phenomena. QCM has been used in combination with CD's as gas phase sensors [27, 28] and aqueous molecular [29, 30] or chirality sensors [31–33]. A monolithic QCM array was operated at multiple frequencies and with various surface coatings, including βCD [34], and showed the potential for parallel sensors in screening applications. A recent study exploited the βCD–adamantane interaction for gene detection using QCM [26]; the detection scheme was based on supramolecular complex formation by ferrocenyl-βCD and adamantylnaphthalene diimide bound to double stranded DNA, where both mass and electrochemical signals were monitored.

With the increasing prevalence of applications based on guest interactions with immobilized βCD, there is a need for greater understanding of the thermodynamics and kinetics of these interactions. In this study, we demonstrate the use of QCM as a tool for examining βCD immobilization and surface host–guest interactions of immobilized βCD with adamantane derivatives. Thermodynamic and kinetic parameters of surface interactions are also presented. The reported data forms the basis for further quantitative study of immobilized βCD interacting with adamantane conjugated to various biomolecules. Surface host–guest kinetic and thermodynamic data are relevant to the customization and optimization of sensory and coupling applications.

QCM background

A basic QCM apparatus consists of a quartz crystal that is coated with a pair of gold electrodes, oscillation circuitry, and a frequency counter. The quartz crystal sensor oscillates at its resonance frequency which is a function of sensor material properties. Mass adsorbed to the surface, Δm, results in a shift in resonance frequency, Δf. Sauerbrey's equation is the most frequently used relationship between these quantities and is strictly valid for uniform, rigid and thin films [35, 36]:

$$\Delta f = -C_f \Delta m \tag{1}$$

C_f, the Sauerbrey constant, is a function of the resonant frequency and crystal properties, and has the values of 56.6 Hz cm^2/μg and 183 Hz cm^2/μg, respectively, for commonly used 5 MHz and 9 MHz quartz AT-cut crystals. QCM measurements of surfaces that do not conform to idealized Sauerbrey assumptions result in deviations in C_f values. Other analyses apply equivalent electrical circuits that model the oscillating mechanics of the sensor/adsorbed mass system. A commonly used model is the Butterworth–van Dyke (BVD) equivalent circuit [37]. Further refinements to the BVD model include specific parameters relating to liquid and mass loading [38] where parametric data are extracted from a network analyzer.

Factors other than mass loading can also influence the QCM response. Liquid loading, or solvent molecules near the crystal surface, and non-rigid or viscoelastic surface layers give rise to resistance shifts and deviations from ideal frequency shifts. Thus, the capabilities of QCM as a gravimetric sensor are least ambiguous for the detection of a rigid, thin film mass-loading under gas-phase conditions [39, 40]. However, it is possible to determine mass contributions for thin-films under liquid loading, provided the added mass satisfies the thin-film criterion. The thin-film criterion implies a zero-phase shift between the top and bottom of the coating [41], and is satisfied if:

$$\varphi_c = 2\pi f_o h_c \sqrt{\frac{\rho_c}{G_c}} \ll \frac{\pi}{2} \tag{2}$$

where f_o is the fundamental frequency, h_c is the film thickness, ρ_c is the density, and G_c is the shear modulus of the coating.

When the thin-film criterion is satisfied, liquid loading and adsorbed mass contributions to QCM crystal motion can be approximated as additive frequency shifts. Martin has presented a model [38] applicable to thin-films which uses the additive nature of frequency shifts due to mass and liquid loading. For example, detection of a 200 nm rubbery coating under liquid loading resulted in only a 10% error in mass using Martin's model [42]. Martin's model should also be applicable to thinner coatings, such as the AD-PEG conjugates in this study.

The electric circuit representation presented by Martin et al. [38] models the unperturbed QCM as an inductance, capacitance, and resistance in series; the liquid loading is represented as an inductance and resistance in series; and

the mass loading is modelled as an inductance. The overall system is represented as the naive QCM crystal, the liquid loading and the mass loading arranged in series. Electrodes and wiring are represented as capacitances in parallel with the crystal, and the liquid and mass loading. With this model, resistance change upon adsorption is attributed solely to changes in liquid loading:

$$\Delta R = \Delta R_{liquid} \qquad (3)$$

and observed change in frequency is attributed to the combination of liquid and mass loadings:

$$\Delta f = \Delta f_{liquid} + \Delta f_{mass} \qquad (4)$$

Δf_{liquid} and ΔR_{liquid} have both been shown to be linearly related to $(\rho_L \eta_L)^{0.5}$, where ρ_L and η_L are the liquid density and viscosity, respectively [38, 43]. It can then be shown that Δf_{liquid} and ΔR_{liquid} are linearly related to each other:

$$\Delta f_{liquid} \approx -\frac{\Delta R_{liquid}}{4\pi L_1} \qquad (5)$$

where L_1 is the free inductance of the unperturbed sensor. For our system, L_1 was independently measured for each experiment to be 0.039 ± 0.003 H, in agreement with 5 MHz chips analyzed using network analyzers [38].

Experimental

Materials

1-Adamantanecarboxylic acid (99%), 1-adamantylamine (97%), 1-adamantanemethylamine (98%), β-cyclodextrin (98%), iodine (99.8%), potassium bisulfate (laboratory grade), sodium hydroxide (97%), sodium methoxide (95%), thiourea (99%), triphenylphosphane (99%), dimethylformamide (DMF, 99.9%), methanol (99.8%) from Sigma/Aldrich, methoxy-poly(ethylene glycol)-N-hydroxysuccinimide (mPEG-NHS, 5000 MW) from Nektar Therapeutics, potassium hydroxide (87.1%) from J.T. Baker, dichloromethane (99.5%) from Caledon Laboratories Ltd, and sulphuric acid (95–98%) from EMD Chemicals Inc., were used as received. Distilled water was further purified with a Nano-pure system: deionized (18.2 M Ω-cm) and filtered through a 0.22 µm filter cartridge. Dimethylsulfoxide (DMSO, 99.9%) from EMD Chemicals Inc. and ethanol (100%) from Commercial Alcohols Inc. were filtered using vacuum filter units (0.22 µm nylon, Corning Inc.) before use.

Synthesis and characterization

Per-6-iodo-β-cyclodextrin and per-6-thio-β-cyclodextrin (t$_7$-βCD) were synthesized, and characterized using a Gemini 300 (300 MHz, Varian) NMR spectrometer. Per-6-iodo-β-cyclodextrin (5.13 g, 71%) was synthesized from β-cyclodextrin (4.32 g) and iodine using a procedure described by Gadelle and Defaye [44] and later modified by Rojas et al. [45] that selectively halogenates the primary hydroxyl groups of CD. ^{1}H NMR (300 MHz, CD$_3$SOCD$_3$) showed the following: δ 3.27–3.49 (m, 21 H, H-2, H-4, H-6a), 3.58–3.69 (m, 14 H, H-3, H-5), 3.82 (d, J = 9.7 Hz, 7H, H-6b), 5.00 (d, J = 2.6 Hz, 7H, H-1), 5.94 (s, 7H, OH-3), 6.04 (d, J = 6.6 Hz, 7 H, OH-2).

Per-6-thio-β-cyclodextrin (t$_7$-βCD, 0.52 g, 82%) was prepared from per-6-iodo-β-cyclodextrin (0.97 g) by a protocol described by Rojas et al. [45]. ^{1}H NMR (300 MHz, CD$_3$SOCD$_3$) showed: δ 2.15 (t, J = 8.2 Hz, 7 H, SH), 2.78 (m, 7 H, H-6a), 3.21 (m, 7 H, H-6b), 3.36–3.40 (m, 14 H, H-2, H-4), 3.63 (t, J = 10 Hz, 7 H, H-3), 3.71 (t, J = 9.7 Hz, 7 H, H-5), 4.96 (s, 7H, H-1), 5.84 (s, 7H, OH-3), 5.94 (d, J = 6.6 Hz, 7H, OH-2).

Adamantane-poly(ethylene glycol) was synthesized from 5,000 Da PEG-NHS using succinimide-amine chemistry in dichloromethane, and purified by dialysis in water using Fisherbrand Regenerated Cellulose Dialysis Tubing (3500 MWCO, Fisher Scientific) following procedures described by Pun and Davis [20]. The purified product was analyzed on a Waters HPLC system with a refractive index detector and a C18 column (Symmetry, 5 µm, 4.6 × 150 mm). Using a 50:50 acetonitrile/water gradient at 0.3 mL/min flowrate, the starting material mPEG-NHS (5.3 min retention time) and product (6.4 min retention time) were well-resolved.

QCM adsorption/desorption and association/dissociation experiments

A QCM (5 MHz, QCM-100, Stanford Research Systems) with attached flow reservoirs and tubing was operated in a 20 L waterbath controlled at 30.00 $\pm$ 0.02 °C (HAAKE DC-30, Thermo Corporation). Liquids were degassed (Waters In-Line Degasser AF), and transported in 1/8″ PTFE tubing using a variable-speed syringe pump (RAZEL A-99). Measurements were taken using a frequency counter (53181A, Agilent) and multimeter (34401A, Agilent). Frequency versus time data were collected during experiments using software (Intuilink, Agilent) for the two devices via GPIB. Polished gold–chromium plated 5 MHz crystals were also from Stanford Research Systems.

QCM crystals were carefully cleaned prior to use. Using a 50 mL PTFE beaker and PTFE-coated tweezers, each crystal was sonicated twice in sulphuric acid (10 mL/3 min), then twice in ethanol (30 mL/20 min). The crystal was then dried under a stream of nitrogen and loaded into the flow cell. t$_7$-βCD (0.015 g) was dissolved in 240 mL of

the DMSO/H_2O mixture to make a 50 µM solution. The remaining DMSO/H_2O from the same batch was used as the blank solution in QCM runs. The solutions were syringed filtered (Pall, 0.22 µm PTFE), degassed, and loaded into the QCM flowlines. The temperature for the water bath was set to 30.00 ± 0.02 °C. When the temperature of the system had stabilized, the blank solution was introduced into the QCM cell at a flowrate of 8.5 mL/h. QCM data were collected every 2 s. Once a minimum of 10 min of flat baseline (±0.5 Hz) was obtained, the t_7-βCD solution was introduced into the QCM cell by actuating a 3-way valve. The t_7-βCD solution was run for 60 min, and then blank solution flow was re-introduced for approximately 45 min.

Using a t_7-βCD coated-sensor in the flowcell, association and dissociation experiments with adamantane-poly(ethylene glycol) (AD-PEG), 1-adamantanecarboxylic acid (AD-C) and 1-adamantylamine (AD-A) were also performed at 30.00 ± 0.02 °C. AD-PEG experiments were performed at an 8.5 mL/h flowrate, while AD-C and AD-A experiments were performed at a 42.5 mL/h flowrate to obtain kinetic data. Nanopure water was used to make 2, 4, 8, 12.5, 25, 50 µM AD-PEG, 500 µM AD-C and 500 µM AD-A solutions, and as the blank solvent. The solutions were syringe filtered and degassed as described above. QCM data were collected every 2 s. Flow-switching between water and AD-PEG, AD-C or AD-A solutions was repeated from three to five times in each run.

XPS surface characterization

After QCM adsorption experiments, CD-adsorbed surfaces were characterized using XPS to confirm the presence of t_7-βCD. X-ray photoelectron spectroscopy (XPS MAX-200, Leybold) was performed using an unmonochromated magnesium K_α source (1253.6 eV), operating at 15 kV and 20 mA. Low resolution scans were conducted at scanning angle of 90° and 20°, and high resolution scans at 20° were conducted to obtained detailed analyses of carbon and sulphur elements. Low resolution spectra (192 eV pass energy) were normalized to unit transmission of the spectrometer, and were subsequently used to determine atomic composition. The sensitivity factors empirically derived by the manufacturer (Au_{4f} = 7.38, O_{1s} = 0.78, C_{1s} = 0.34 and, S_{2p} = 0.84) were used [46]. High resolution spectra (48 eV pass energy) were fitted (ESCATools, Surface/Interface Inc.) to obtain more detailed chemical information. Uncoated electrodes were subjected to the same washing procedure as the coated electrodes, and used as controls.

Results and discussion

Self-assembly of t_7-βCD on gold

QCM

Figure 1 shows the QCM frequency and resistance output from a typical adsorption/desorption experiment of t_7-βCD on gold. Each experiment begins with the flow of DMSO/H_2O solvent until a flat baseline (±0.5 Hz) is obtained for 10 min. Flow is then switched to introduce t_7-βCD solution into the flowcell; the flow switch introduces an immediate decrease in frequency most likely due to a slight mismatch in pressures between the two lines. After a lag period, the t_7-βCD solution front reaches the sensor position, and a sharp decrease in frequency is observed, signalling the onset of t_7-βCD adsorption onto the gold surface. The frequency decrease continues until a plateau is reached which typically occurs in about 20–30 min, indicating saturation between the surface and the solution. Upon switching back to the solvent, the resonant frequency increases after a lag period, and typically stabilizes at an intermediate value within 10–15 min. As indicated by Δf_{rev} and Δf_{irr} in Fig. 1, the QCM scans show the presence of both reversibly and irreversibly adsorbed t_7-βCD. Concomitant with frequency shifts, electrical resistance increased with adsorption, and decreased upon desorption of t_7-βCD.

For the deposition of t_7-βCD, a rigid 1-nm coating, the condition for the thin-film assumption (Eq. 2) is readily satisfied. Adopting Martin's approach, Eqs. 3–5 were used to determine Δf_{mass} from ΔR_{irr} and Δf_{irr} from seven t_7-βCD adsorption experiments. Irreversibly adsorbed mass Δm was then calculated using Eq. 1. It was found that for the irreversibly adsorbed fraction: $\Delta f_{mass} = 5.06 \pm 0.19$ Hz and $\Delta m = 7.17(\pm 0.27) \times 10^{-11}$ mol/cm^2 = $8.95(\pm 0.34) \times 10^{-8}$ g/cm^2.

Thiol groups on t_7-βCD enable the self assembly of a layer of βCD molecules onto the gold surface. The synthesis conditions ensure that the thiol groups were introduced on the primary face of CD [44]; it was therefore anticipated that t_7-βCD would assemble onto the gold electrode in a single layer with the larger end of the torus exposed to facilitate subsequent interactions with guest molecules. The QCM frequency readings plateaued during t_7-βCD adsorption (Fig. 1) indicating surface saturation. Subsequent desorption with solvent contact showed that a fraction of the adsorbed t_7-βCD is reversibly adsorbed. t_7-βCD has a molecular diameter of 15.4 Å, and an area of 186.3 $Å^2$ [3]. A close-packed monolayer of t_7-βCD molecules on a surface would have an approximate surface coverage of 8.92×10^{-11} mol/cm^2, corresponding to a 6.3 Hz frequency shift for an idealized C_f value of 56.6 Hz cm^2/µg.

Fig. 1 QCM signal profiles from a typical t_7-βCD adsorption/desorption experiment. Flow switching points from solvent to t_7-βCD solution (1) and back to solvent (2) are indicated. Also shown are the irreversible shifts in frequency and resistance, Δf_{irr} and ΔR_{irr}, as well as the reversible frequency shift Δf_{rev}
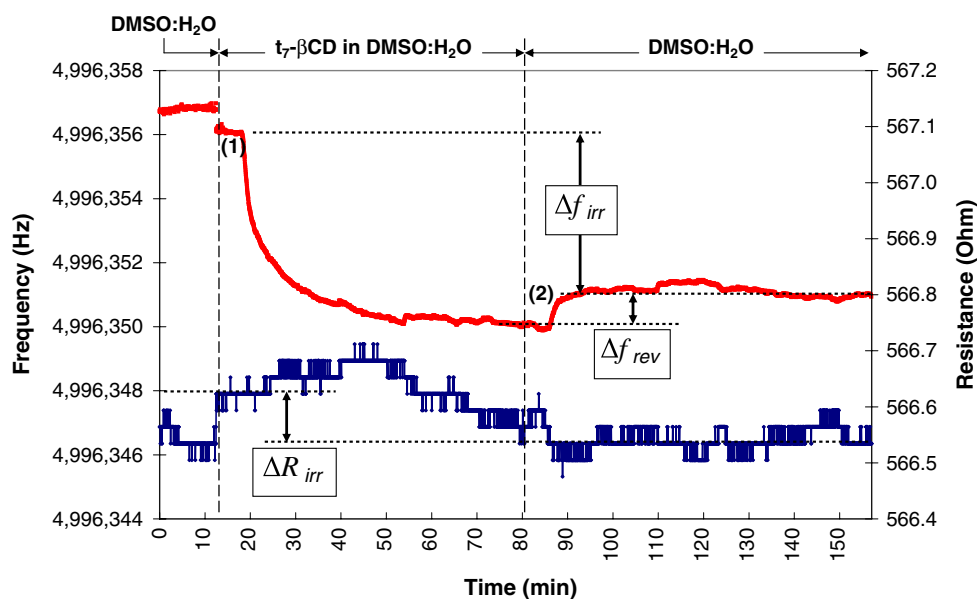
Using these parameters, the measured irreversibly adsorbed surface concentration corresponds to 80 ± 3% of a close-packed monolayer. Reversibly adsorbed t_7-βCD may include molecules that are loosely adhered to the surface in gaps between tightly adsorbed t_7-βCD, or t_7-βCD that aggregates with irreversibly adsorbed t_7-βCD through hydrogen bonding via the rim hydroxyl groups [47].

A number of researchers have reported similar surface coverage of t_7-βCD on gold. Rojas et al. [45] and D'Annibale et al. [48] both used a reductive desorption technique to obtain surface coverages of 64–75% and 80 ± 6%, respectively. Liu et al. [49] coated gold nanoparticles with t_7-βCD and dissolved the gold to determine a t_7-βCD surface coverage of 75 ± 9%. Contradictory results were reported by Lee and Park [50] who used an electrochemical QCM to obtain surface coverages of 150% from the adsorption frequency shift and 107% from reductive desorption, and speculated that gold electrode surface roughness may have been the reason for the apparent super-monolayer coverage. So aside from Liu's anomalous result, the t_7-βCD adsorption results presented in this study are in agreement with reported literature.

XPS

Sensor chips after t_7-βCD adsorption experiments were analyzed by XPS to confirm t_7-βCD coating. Low resolution XPS data (Table 1) show higher carbon and sulphur, and lower gold content for coated electrodes relative to controls. Furthermore, relative to 90° scans, the shallower sampling depth of 20° scans gave lower measured gold content for both control and coated electrodes, and higher

sulphur content for the coated electrodes. These results are consistent with t_7-βCD coating on an underlying gold substrate. Binding energies for carbon and sulphur from 20° high resolution scans are shown in Table 2. Sulphur data indicate only one bond type; the 163.6 eV/164.78 eV p-orbital doublet corresponding to S–C bonds [51, 52]. Carbon data show 55% bond character at 284.5 eV typically attributed to elemental carbon, C–C, and C–H bonds, and 34% bond character at 286.3 eV typically known for C–O bonds [51]. While CD molecules include both types

Table 1 Low resolution XPS

Element	Control electrode		Coated electrode	
	90°	20°	90°	20°
Carbon (1s) (%)	37.4	53.4	49.6	61.0
Oxygen (1s) (%)	29.0	39.4	21.4	28.3
Sulphur (2p) (%)	0.0	0.0	2.3	3.6
Gold (4f) (%)	33.6	7.3	26.6	7.1

Table 2 High resolution XPS at 20°

Carbon: FWHM[a] = 1.50 eV			Sulphur: FWHM[a] = 1.65 eV		
Orbital	Centre (eV)	Area %	Orbital	Centre (eV)[b]	Area %[b]
1s	284.47	55.0	2p 3/2	163.60	66.7
1s	286.25	33.7	2p 1/2	164.78	33.3
1s	287.91	11.3			

[a] Full width at half maximum

[b] Spin multiplicity restricts energy shift = 1.18 eV and relative areas between orbitals

[c] Peak fit using a Gauss/Lorentz function (20% Lorentz)

of bonds, these bonds are common and their presence does not provide definitive proof of surface composition. Carbon data also show 11.3% bond character at 287.9 eV. t_7-βCD molecules include C–S and O–C–O moieties both of which have carbon binding energies at 287.9 eV [51]. t_7-βCD molecules have equal ratios of C–S and O–C–O bonds, so each bond type should contribute half of the bond character at this energy. With carbon comprising 61% atomic composition from 20° low resolution scans, it can be directly inferred that carbon in C–S bonds comprise ∼3.4% of the surface atomic composition, consistent with the 3.6% sulphur content observed in the same scan. The XPS data thus provide strong evidence of t_7-βCD adsorption on gold sensors to support QCM results.

Fig. 2 QCM Profiles of AD-PEG and PEG association and dissociation profiles on t_7-βCD coated surfaces. 50 μM solutions of AD-PEG and PEG profiles are shown in green and blue, respectively

Inclusion of adamantane derivatives with immobilized t_7-βCD

After t_7-βCD adsorption/desorption in 60:40 DMSO/H$_2$O, the flowcell was purged with air, then flow was switched to water and aqueous adamantane derivative solutions for complexation experiments.

AD-PEG complexation with immobilized t_7-βCD

The association and dissociation of AD-PEG from solution onto t_7-βCD coated surfaces resulted in reversible shifts in frequency and resistance. QCM data from AD-PEG inclusion experiments were analyzed according to Martin's model to isolate frequency shifts due to adsorbed mass. Data processed in this manner from a representative inclusion experiment is shown in Fig. 2. From a 50 μM AD-PEG solution, a 17 Hz reversible association interaction was observed. Figure 2 also includes results from a control experiment conducted with a 50 μM PEG-5000 solution which resulted in minimal (<1 Hz) association between PEG-5000 and the t_7-βCD coated surface. It is evident that the AD/CD complexation interaction is the mechanism that drives AD-PEG association onto a t_7-βCD coated surface. AD-PEG inclusion experiments were conducted at a flowrate of 8.5 mL/h. Under these
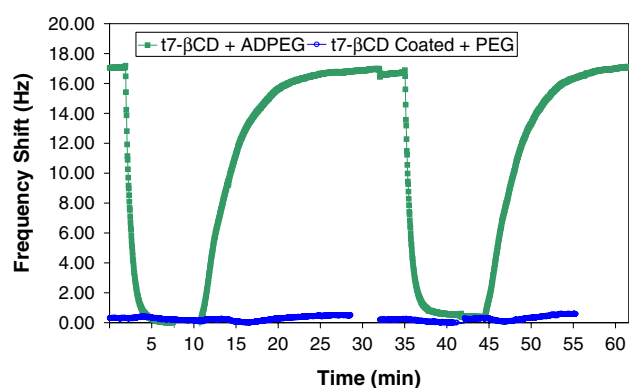
conditions, association was mass transfer-limited, thus intrinsic association kinetic parameters could not be extracted. Much higher flowrates were required to be in an association kinetics-controlled regime, which would have required much larger amounts of AD-PEG. The frequency shift results for AD-PEG inclusion obtained after applying the Martin model, and the corresponding surface concentrations, are summarized in Table 3 for AD-PEG concentrations ranging from 2 to 50 μM. Fraction surface coverage θ_{eq} values were calculated relative to t_7-βCD surface coverage, i.e. 100% occupancy of surface adsorbed t_7-βCD was taken as full surface coverage of AD-PEG. Table 3 shows that frequency shifts and surface concentrations increase with increasing AD-PEG concentrations.

The association behaviour can be described by a Langmuir isotherm:

$$\frac{\Delta f}{\Delta f_{max}} = \theta_{eq} = \frac{CK}{1 + CK} \qquad (6)$$

where Δf is the frequency shift, Δf_{max} is the maximum or saturation frequency shift, θ_{eq} is the fractional coverage in equilibrium with the bulk concentration C, and K is the equilibrium constant. The data in Table 3 were fitted using Origin Pro 7.5 (OriginPro Corporation) for reduced χ^2 using the Levenberg–Marquardt method to obtain the best

Table 3 AD-PEG association on a t_7-βCD surface

AD-PEG concentration (μM)	Δf_{mass} (Hz)	Δm (ng/cm^2)	Δm (pmol/cm^2)	θ_{eq}
2	4.70 ± 0.61	83.1 ± 10.7	15.53 ± 2.00	0.23 ± 0.03
4	6.90 ± 0.45	121.9 ± 7.9	22.79 ± 1.48	0.31 ± 0.02
8	9.30 ± 0.64	164.4 ± 11.4	30.74 ± 2.12	0.44 ± 0.03
12.5	11.34 ± 1.28	200.4 ± 22.7	37.46 ± 4.24	0.52 ± 0.06
25	14.22 ± 1.15	251.2 ± 20.3	46.96 ± 3.79	0.66 ± 0.05
50	17.36 ± 1.12	306.8 ± 19.8	57.36 ± 3.70	0.80 ± 0.05

fit parameters $K = 125,000 \pm 18,000$ M^{-1} and $\Delta f_{max} = 19.5 \pm 1.0$ Hz (Fig. 3). From the best fit frequency value, the calculated saturated surface mass concentration is 344.5 ± 17.7 ng/cm^2.

Studies of the AD/βCD interaction have generally shown the complexation to be strong, but reversible. de Jong et al. [53] studied the complexation of 1-acetamido-adamantane with βCD. Using SPR, the equilibrium constant K for the interaction between immobilized βCD and AD in solution was found to be 57,000 M^{-1}. A value of 65,000 M^{-1} was found using microcalorimetry when both species were in solution. In a different approach, Brown et al. [54] obtained $K = 28,000$ M^{-1} for the complexation between immobilized tethered-AD and βCD in solution using SPR. In both studies, complexation could be reversed by returning to blank solvents.

Some variants of the AD-PEG/βCD system have been studied by Millot and coworkers [21, 23, 55, 56]. In a series of experiments, primarily with adamantylphenyl-PEG (5000 MW) interacting with immobilized poly-βCD, the K values reported ranged from 400 [56] to 5,000 M^{-1} [23]. It is significant that the poly-βCD bound AD-PEG derivatives did not elute when contacted with water: irreversible association was observed by SPR [21] or by affinity high performance liquid chromatography where AD-PEG did not elute from the polyβCD column [55]. The observed irreversibility of complexation between AD-PEG and polyβCD is difficult to reconcile with the reported range of K values. Near irreversible binding of the biotin–avidin interaction has $K \approx 10^{15}$ M^{-1} [57], and the K values of reversible AD/βCD interactions are in the 28,000–65,000 M^{-1} range [53, 54].

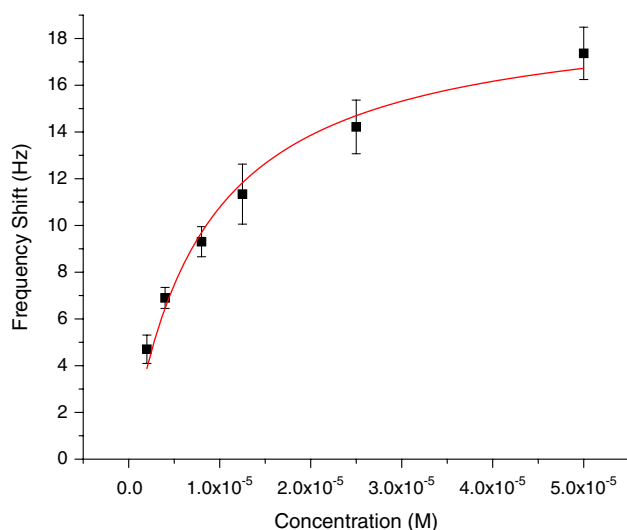**Fig. 3** Frequency shift versus bulk AD-PEG concentration data. Best-fit Langmuir isotherm parameters: $\Delta f_{max} = 19.5 \pm 1.0$ Hz and $K = 125,000 \pm 18,000$ M^{-1}

The best-fit K value of 125,000 M^{-1} obtained in this study is higher than the 57,000 M^{-1} [53] found by de Jong for AD with immobilized βCD. It is possible that the stronger inclusion interaction seen in this study is due to the conformation of the protruding PEG chains. The hydrodynamic radii of PEG$_{4000}$ and PEG$_{6000}$ were reported to be 1.9 and 2.5 nm, respectively [58], while βCD has a radius of 0.7 nm [3]. The binding area of an AD-PEG (PEG: 5,000 MW) molecule exceeds the area of an immobilized t$_7$-βCD molecule. It is plausible that the overlapping hydrodynamic radii of immobilized AD-PEG lead to entangled PEG chains. Entanglement should stabilize bound complexes by preventing desorption and thus give higher K values. Entangled PEG chains may also have been a contributing factor to the irreversible association reported by Millot and coworkers [21, 55].

As the PEG control association showed, the association of AD-PEG to the surface is due to the AD/t$_7$-βCD interaction, thus the maximum molar surface concentration of AD-PEG should be the same as the surface concentration of CD, or 71.7 ± 2.7 pmol/cm^2, or 5.06 ± 0.19 Hz QCM signal. On this basis, AD-PEG should generate a theoretical maximum frequency shift of 21.7 ± 0.8 Hz for 1-to-1 inclusion to t$_7$-βCD and complete coverage. The fitted results from experimental data indicate the maximum to be $f_{max} = 19.5 \pm 1.0$ Hz. While the difference is relatively small, the lower experimental value suggests surface saturation and/or inaccessible surface sites leading to a smaller f_{max}.

Steric effects may contribute to incomplete surface coverage between βCD and AD-PEG. As discussed above, the hydrodynamic radius of the PEG chain is larger than the radius of βCD. Entangled PEG chains may cause steric obstruction and would lead to a sub-saturation value of f_{max}.

It is worthwhile to examine the validity of the thin-film assumption underlying the data analysis presented above. Five t$_7$-βCD coated sensor chips were used for AD-PEG inclusion studies. All six concentrations of AD-PEG solutions were run on each chip, iterating three association/dissociation cycles for each concentration. For each concentration, no trends or notable differences were observed between chips, so data at each concentration from all chips can be grouped. In Fig. 4, the frequency shift (Δf) and resistance shift (ΔR) for association/dissociation cycles is plotted for each concentration. An increase in concentration results in an increase in frequency and resistance shift. The decreases in frequency are linear with respect to the increases in resistance, and for all tested concentrations, the plots align along approximately the same slope.

Association of AD-PEG generates a shift in frequency, while the water associated with PEG gives rise to shifts in both frequency and resistance. The slope of the lines in
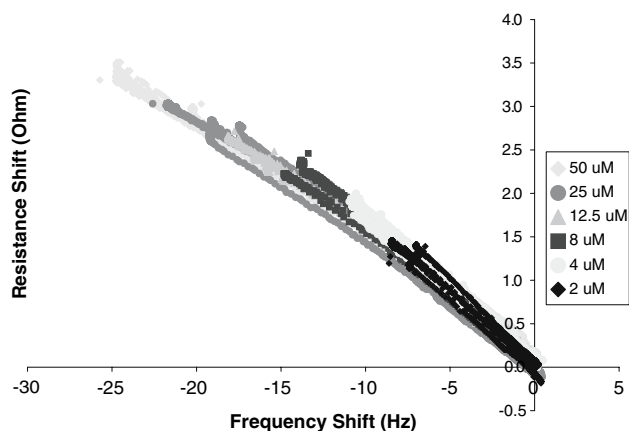
Fig. 4 Δf –ΔR Chart for AD-PEG association/dissociation at various concentrations. Each concentration is comprised of representative data from five QCM chips

Fig. 4, $\Delta R/\Delta f$, relates to the viscoelastic properties (G′/G″) of the bound mass [41]. Figure 4 shows that bound AD-PEG shows a constant material property throughout the association process for all solution concentrations used. Since interpretation of QCM signals is difficult when surface interactions occur in combination with changing film properties, Figure 4 validates the thin-film assumption that underlies the analysis of the QCM data, and thus provides supporting validation for the fitted values of Δf_{max} and K.

Immobilized t₇-βCD complexation kinetics for AD-C and AD-A

A typical QCM scan from an association/dissociation kinetic experiment is shown in Fig. 5. Similar to AD-PEG association/dissociation profiles, flow switches between AD-C or AD-A (herein referred to as ligand) solutions and water resulted in frequency changes that are indicative of either complexation between the adamantane species and
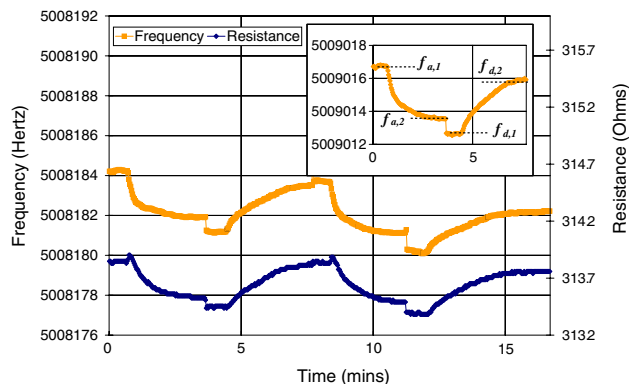

Fig. 5 QCM profile of AD-C association/dissociation onto t₇-βCD immobilized on a 5 MHz sensor. The inset graph is the frequency profile after applying Martin's model to isolate mass contribution

immobilized t₇-βCD, or dissociation of the complex. The reversibility of the process allowed up to five association/dissociation cycles within a single run.

In contrast to the opposing frequency and resistance changes seen in t₇-βCD adsorption/desorption (Fig. 1) and AD-PEG/βCD association/dissociation (Fig. 4), frequency and resistance decreased or increased in parallel during t₇-βCD and AD-C or AD-A association/dissociation (Fig. 5).

To determine the conditions which there are mass transfer limitations interfering with adsorption kinetics, experiments were first conducted at flowrates that ranged from 8.5 to 46.5 mL/h. At low flowrates, the association profile appeared linear with time, indicative of a mass-transfer-limited process. Increasing flowrates resulted in increasingly non-linear appearance of association profiles. The observed adsorption did not change significantly with flowrates above 42.5 mL/h, indicating that association was kinetically limited, thus all subsequent experiments were conducted at 42.5 mL/h.

The time dependence of the fractional surface coverage of the ligand/t₇-βCD complex $\theta(t)$ can be written as,

$$\frac{d\theta}{dt} = Ck_a(1 - \theta(t)) - k_d\theta(t) \tag{7}$$

where C is the ligand concentration in solution and k_a and k_d are the association and dissociation rate constants, respectively.

The time-independent solution of Eq. 7 gives the Langmuir isotherm, Eq. 6, or with $K = k_a/k_d$, $\theta_{eq} = (Ck_a)/(Ck_a + k_d)$

Equation 7 can be solved for the association phase (at $t = 0$, $\theta = 0$), and the dissociation phase ($C = 0$, and at $t = 0$, $\theta = \theta_{eq}$). Combining the solutions with Sauerbrey's equation (Eq. 1) give relationships between frequency shifts and surface coverage.

During the association phase:

$$\begin{aligned} \Delta f(t) &= C_f\Delta m = C_f n_{max}M\theta(t) \\ &= C_f n_{max}M\theta_{eq}(1 - exp(-(Ck_a + k_d)t)) \end{aligned} \tag{8}$$

where $\Delta f(t)$ is the frequency shift attributable to bound mass relative to the baseline frequency at the beginning of the association phase, n_{max} is the maximum molar surface coverage of AD-C or AD-A, equivalent to the molar concentration of immobilized t₇-βCD, and M is the apparent molar mass of the ligand.

During the dissociation phase:

$$\Delta f(t) = C_f\Delta m = C_f n_{max}M\theta(t) = C_f n_{max}M\theta_{eq}(exp(-k_dt)) \tag{9}$$

where $\Delta f(t)$ is the frequency shift attributable to bound mass relative to the end of the dissociation phase when all reversibly bound ligand have been released from the surface.

The frequency and resonance shifts obtained from QCM runs were analyzed using Eqs. 3–5 as before to isolate the frequency shift due to mass loading from ligand binding, then analyzed according to Eqs. 8 and 9 to extract kinetic rate constants and equilibrium constants. $t = 0$ was set visually to the onset of frequency signals, and association and dissociation profiles were fit using Origin Pro 7.5 (OriginPro Corporation) for reduced χ^2 using the Levenberg–Marquardt method to obtain best fit parameters. Two parameter fit of association and dissociation profiles give values for k_d from Eq. 9, and $k_aC + k_d$ from Eq. 8, from which k_a can be calculated. Use of Eq. 6 to determine θ_{eq} allowed the subsequent calculation of M.

Immobilized t_7-βCD complexation kinetics with AD-C

Four experimental runs were made at 42.5 mL/h using a 500 μM AD-C solution (pH 4.2). The rate constants were found to be $k_a = 100 \pm 5$ $M^{-1}\,s^{-1}$ and $k_d = 110\,(\pm18) \times 10^{-4}\,s^{-1}$, and the apparent molar mass M was found to be 775 g/mol. A consistency check of the association rate constant was obtained from early time association kinetics data where:

$$\left(\frac{df}{dt}\right)_{o,a} = C_f n_{max} M \left(\frac{d\theta}{dt}\right)_{o,a} \qquad (10)$$
$$= C_f n_{max} M C k_a (1 - \theta(t)) \approx C_f n_{max} M C k_a$$

The association rate constant k_a obtained from the same runs, using $M = 775$ g/mol from above, was 93 ± 8 $M^{-1}\,s^{-1}$, consistent with the best fit value of 100 ± 5 $M^{-1}\,s^{-1}$ reported above. The equilibrium constant is then $9,400 \pm 1,700$ M^{-1}. Results are summarized and compared to literature data in Table 4.

Only one kinetic study of AD-C association to immobilized t_7-βCD is available for comparison of kinetic parameters. Busse et al. [59] immobilized βCD to a silicon oxynitride surface via short spacers and used a Mach–Zehnder interferometer to measure complexation kinetics. From 500 μM AD-C in PBS, k_a and k_d were found to be 144 $M^{-1}\,s^{-1}$ and 0.027 s^{-1}, respectively, resulting in $K = 5,300$ M^{-1}. Differences in experimental conditions with this study include spacer length, and solvent. AD-C dissolved in pH 7 PBS would have a different proportion of ionized species compared to AD-C at pH 4.2 as used in this study. The difference in solution pH may also result in kinetics-altering effects, such as surface charging. In spite of these differences, Busse's association and dissociation constants are the same order of magnitude as the rate constants obtained in this study.

Impedance spectroscopy was used by Michalke et al. [60] to obtain an AD-C/βCD equilibrium constant. βCD was immobilized via spacers, and AD-C solutions were prepared at pH 8.0 to ensure fully charged guest species for inclusion. The equilibrium constant found was $K = 2,400$ M^{-1}. AD-C data are tabulated in Table 4 for comparison.

The pK_a of AD-C is approximately 5, and increasing pH would result in greater deprotonation of the carboxylic acid moiety. As shown in Table 4, the equilibrium constant of complexation between AD-C and immobilized βCD reported in three different studies decreases as bulk solution pH increases. Ionized adamantane derivatives have a greater affinity for water, and repulsive forces may limit the surface coverage of ionized species; these two factors would result in a lower equilibrium constant. The reported AD-C equilibrium data are consistent with this explanation.

Immobilized t_7-βCD complexation kinetics with AD-A

Four experimental runs were made at 42.5 mL/h using a 500 μM AD-A solution in water (pH 10.2). The extracted rate constants found were $k_a = 58.2 \pm 5.9$ $M^{-1}\,s^{-1}$ and $k_d = 154\,(\pm7) \times 10^{-4}\,s^{-1}$, respectively, and the M was found to be 2,190 g/mol. The calculated equilibrium constant is $K = (k_a)/(k_d) = 3800 \pm 400\,M^{-1}$. The results are summarized in Table 4.

Interactions between immobilized βCD and adamantanamine hydrochloride (AD-AHC) have been studied by Michalke et al. [60] using impedance spectroscopy. Buffered solutions of AD-AHC solution at pH 5.5 were prepared to ensure fully charged guest species, AD-NH$_3^+$. The equilibrium constant found was $K = 13,000$ M^{-1}, and is included in Table 4 for comparison.

Table 4 Association, dissociation and equilibrium constants between adamantane derivatives and immobilized βCD

	Species	pH	k_a ($M^{-1}\,s^{-1}$)	k_d (s^{-1})	K (M^{-1})
Poon (this study)	AD-COOH/AD-COO$^-$	4.2	100 ± 5	$110\,(\pm18) \times 10^{-4}$	$9,400 \pm 1,700$
Busse et al. [59]	AD-COOH/AD-COO$^-$	7	144	270×10^{-4}	5,300
Michalke et al. [60]	AD-COOH/AD-COO$^-$	8.0			2,400
Poon (this study)	AD-A/AD-NH$_3^+$	10.2	58.2 ± 5.9	$(154 \pm 7) \times 10^{-4}$	$3,800 \pm 400$
Michalke et al. [60]	AD-AHC/AD-NH$_3^+$	5.5			13,000

The pK$_b$ of AA is approximately 4.2. As the pH of AA solutions decreases, the amine moiety becomes increasingly protonated as A-NH$_3^+$. As with AD-C, increasing ionization of AD-A should result in a lower equilibrium constant. Michalke's AD-AHC result and the result for AD-A from this study contradict the expected trend. QCM is sensitive to charged molecules at the surface, so the difference in counterions used in the two studies, Cl$^-$ in Michalke's study compared to OH$^-$ in the current study, may be the reason for the unexpected equilibrium constant versus pH trend between the two studies.

AD-A and AD-C QCM non-idealities

The detection of molecules onto QCM sensors has been known to be affected by the binding of charged species, often leading to amplified signals [61–64]. As noted before, in order to interpret a QCM response, the film properties are typically considered and the resistance profile monitored. During the adsorption of t$_7$-βCD onto gold and association of AD-PEG to t$_7$-βCD, increased surface mass generated an increase in resistance. The thin-film criterion was verified and Martin's model was therefore applied to obtain gravimetric data. The data for the adsorption of t$_7$-βCD, and AD-PEG association/dissociation experiments generated results that correlated well with literature and theory. In both cases, the inclusion species were uncharged in a pH neutral solvent.

The association/dissociation profiles of AD-C and AD-A with immobilized t$_7$-βCD (see Fig. 5) showed an unusual resistance shift: decreases in frequency were accompanied with decreases in resistance. This phenomenon has been observed in other studies [65, 66], and models have been developed to explain this using interfacial slip [67, 68]. It is beyond the scope of this paper to investigate the mechanism for a binding mass leading to a decrease in resistance. Under these circumstances, there is no *direct* relationship between frequency and mass, as the frequency becomes an unknown combination of gravimetric and non-gravimetric responses [39, 40]. However, a linear correlation has been reported between mass increase and frequency shift for the binding of analytes on coated surfaces [40]. The linear correlation suggests that the binding of analyte corresponds to a consistent proportional increase of gravimetric and non-gravimetric effects. Consequently, mass binding generates an amplified frequency response, and this behaviour is observed in our data.

The association/dissociation profiles for AD-A and AD-C show that the resistance response mimics the frequency response. In Fig. 6, the frequency shift is plotted against the resistance shift, and exhibits a linear correlation. Figures 4 and 6 is the same plot (but different quadrant) as
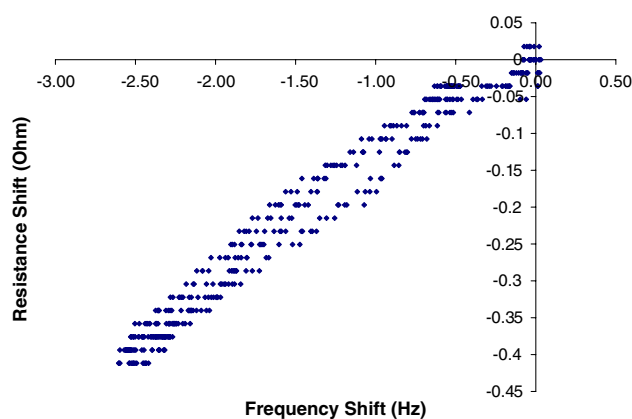

Fig. 6 $\Delta f - \Delta R$ chart for association and dissociation of AD-C from Fig. 5

Fig. 4, exhibiting a linear trend of a different slope. This behaviour indicates a consistent ratio of gravimetric to non-gravimetric response for guest association/dissociation. The fitting results for M have resulted in masses of 775 g/mol for AD-C and 2190 g/mol for AD-A species, and are larger than the theoretical expected results for the molecular masses of AD-C and AD-A of 180.25 g/mol and 151.25 g/mol, respectively. The exaggerated molecular masses are the result of an amplified signal, consistent with the behaviour described by Lucklum et al. [40].

In the association/dissociation experiments, the frequency response cannot be used to directly quantify mass. However, as the frequency increase is proportional to mass increase, surface kinetics can be extracted. The results from the adsorption of t$_7$-βCD indicate the number of surface sites, and the profiles from the association/dissociation experiments show a saturable response. Scaling the saturable response of the association/dissociation experiments to the number of surface sites enables the estimation of mass association/dissociation for the extraction of surface kinetics.

Conclusion

QCM has been used to study the real-time self-assembly of t$_7$-βCD on gold, the binding isotherm for AD-PEG, and the association/dissociation kinetics of AD-C or AD-A with immobilized t$_7$-βCD. Kinetic, thermodynamic, and gravimetric data have been obtained, and compare well to existing literature data. In a single platform, QCM provided characterization of t$_7$-βCD assembly on gold, as well as the subsequent association/dissociation interactions of ligands with t$_7$-βCD. In particular, QCM is one of the few mainstream tools available to contribute to the scarce literature on surface kinetics. QCM provides an inexpensive and quick to assemble platform to further study surface host–

guest kinetic and thermodynamic interactions of immobilized t_7-βCD with various conjugated AD species including amino acids, nucleic acids, and/or biopolymers, and is a valuable tool to advance sensory and coupling applications.

References

1. Crini, G., Morcellet, M.: Synthesis and applications of adsorbents containing cyclodextrins. J. Sep. Sci. **25**(13), 789–813 (2002)

2. Rekharsky, M.V., Inoue, Y.: Complexation thermodynamics of cyclodextrins. Chem. Rev. **98**(5), 1875–1917 (1998)

3. Szejtli, J.: Cyclodextrin Technology. Kluwer Academic Publishers (1988)

4. Eastburn, S.D., Tao, B.Y.: Applications of modified cyclodextrins. Biotechnol. Adv. **21**(2), 325–339 (1994)

5. Gubitz, G., Schmid, M.G.: Recent advances in chiral separation principles in capillary electrophoresis and capillary electrochromatography. Electrophoresis **25**(23–24), 3981 (2004)

6. Chmurski, K., Temeriusz, A., Bilewicz, R.: Beta-cyclodextrin-based ferrocene-imprinted gold electrodes. Anal. Chem. **75**(21), 5687–5691 (2003)

7. Yang, Y., Yang, H.-F., Liu, Y.-L., Liu, Z.-M., Shen, G.-L., Yu, R.-Q.: Cetyltrimethylammonium assay using fluorescence probe berberine and a competitive host-guest complexation with butylated beta-cyclodextrin. Sens. Actuators B Chem. **106**(2), 632–640 (2005)

8. Yang, R.-H., Wang, K.-M., Xiao, D., Yang, X.-H., Zhang, L.-D.: A selective sensing membrane for the determination of tetracycline with heptakis (2,6-di-o-isobutyl)-beta-cyclodextrin as the substrate. Microchem. J. **64**(3), 213–220 (2000)

9. Tanabe, T., Touma, K., Hamasaki, K., Ueno, A.: Fluorescent cyclodextrin immobilized on a cellulose membrane as a chemosensor system for detecting molecules. Anal. Chem. **73**(8), 1877–1880 (2001)

10. Litwiler, K.S., Catena, G.C., Bright, F.V.: Simple fiber-optic sensor based on immobilized beta-cyclodextrin. Anal. Chim. Acta **237**(2), 485–490 (1990)

11. Medintz, I.L., Anderson, G.P., Lassman, M.E., Goldman, E.R., Bettencourt, L.A., Mauro, J.M.: General strategy for biosensor design and construction employing multifunctional surface-tethered components. Anal. Chem. **76**(19), 5620–5629 (2004)

12. Rudzinski, C.M., Young, A.M., Nocera, D.G.: A supramolecular microfluidic optical chemosensor. J. Am. Chem. Soc. **124**(8), 1723–1727 (2002)

13. Atwood, J.L., Lehn, J.: Comprehensive Supramolecular Chemistry. Pergamon, Oxford (1996)

14. Lantz, A.W., Rodriguez, M.A., Wetterer, S.M., Armstrong, D.W.: Estimation of association constants between oral malodor components and various native and derivatized cyclodextrins. Anal. Chim. Acta **557**(1–2), 184–190 (2006)

15. Du, X.Z., Lu, W.H., Ding, N., Dai, H.X., Teng, X.L., Deng, H.L.: Spectral properties and supramolecular inclusion complexes of beta-cyclodextrin with flexible amphiphilic and rigid compounds. J. Photochem. Photobiol. A Chem. **177**(1), 76–82 (2006)

16. Rundlett, K.L., Armstrong, D.W.: Methods for the determination of binding constants by capillary electrophoresis. Electrophoresis **22**(7), 1419 (2001)

17. Zhang, B., Breslow, R.: Enthalpic domination of the chelate effect in cyclodextrin dimers. J. Am. Chem. Soc. **115**(20), 9353–9354 (1993)

18. Bellocq, N.C., Kang, D.W., Wang, X. Jensen, G.S., Pun, S.H., Schluep, T., Zepeda, M.L., Davis, M.E.: Synthetic biocompatible cyclodextrin-based constructs for local gene delivery to improve cutaneous wound healing. Bioconjug. Chem. **15**(6), 1201–1211 (2004)

19. Bellocq, N.C., Pun, S.H., Jensen, G.S., Davis, M.E.: Transferrin-containing, cyclodextrin polymer-based particles for tumor-targeted gene delivery. Bioconjug. Chem. **14**(6), 1122–1132 (2003)

20. Pun, S.H., Davis, M.E.: Development of a nonviral gene delivery vehicle for systemic application. Bioconjug. Chem. **13**(3), 630–639 (2002)

21. David, C., Millot, M.C., Sebille, B., Levy, Y.: The reversible binding of hydrophobically end-capped poly(ethylene glycol)s to poly-beta-cyclodextrin-coated gold surfaces: a surface plasmon resonance investigation. Sens. Actuators B Chem. **90**(1–3), 286–295 (2003)

22. Wintgens, V., Amiel, C.: Surface plasmon resonance study of the interaction of a beta-cyclodextrin polymer and hydrophobically modified poly(n-isopropylacrylamide). Langmuir **21**(24), 11455–11461 (2005)

23. Guerrouache, M., Karakasyan, C., Gaillet, C., Canva, M., Millot, M.C.: Immobilization of a functionalized poly(ethylene glycol) onto beta-cyclodextrin-coated surfaces by formation of inclusion complexes: application to the coupling of proteins. J. Appl. Polym. Sci. **100**(3), 2362–2370 (2006)

24. Cao, R., Villalonga, R., Fragoso, A.: Towards nanomedicine with a supramolecular approach: a review. IEE Proc. Nanobiotechnol. **152**(5), 159–164 (2005)

25. David, C., Millot, M.C., Renard, E., Sebille, B.: Coupling of antibodies to beta-cyclodextrin-coated gold surfaces via an intermediate adamantyl-modified carboxymethylated dextran layer. J. Incl. Phenom. Macrocycl. Chem. **44**(1–4), 369–372 (2002)

26. Sato, S., Nojima, T., Takenaka, S.: Electrochemical gene detection based on supramolecular complex formation by ferrocenyl-beta-cyclodextrin and adamantylnaphthalene diimide bound to double stranded DNA. J. Organometall. Chem. **689**(25), 4722–4728 (2004)

27. Palaniappan, A., Li, X., Tay, F.E.H., Li, J., Su, X.: Cyclodextrin functionalized mesoporous silica films on quartz crystal microbalance for enhanced gas sensing. Sens. Actuators B Chem. **119**(1), 220–226 (2006)

28. Schofield, W.C.E., McGettrick, J.D., Badyal, J.P.S.: A substrate-independent approach for cyclodextrin functionalized surfaces. J. Phys. Chem. B **110**(34), 17161–17166 (2006)

29. Dickert, F.L., Tortschanoff, M., Weber, K., Zenkel, M.: Process control with mass-sensitive chemical sensors - cyclodextrin modified polymers as coatings. Fresenius J. Anal. Chem. **362**(1), 21–24 (1998)

30. Sun, H., Zhang, Y.Y., Si, S.H., Zhu, D.R., Fung, Y.S.: Piezoelectric quartz crystal (PQC) with photochemically deposited nano-sized Ag particles for determining cyanide at trace levels in water. Sens. Actuators B Chem. **108**(1–2), 925–932 (2005)

31. Fietzek, C., Hermle, T., Rosenstiel, W., Schurig, V.: Chiral discrimination of limonene by use of beta-cyclodextrin-coated quartz-crystal-microbalances (QCMs) and data evaluation by artificial neuronal networks. Fresenius J. Anal. Chem. **371**(1), 58 (2001)

32. May, I.P., Byfield, M.P., Lindstrom, M., Wunsche, L.F.: Chiral discrimination using a quartz crystal microbalance and comparison with gas chromatographic retention data. Chirality **9**(3), 225 (1997)

33. Ng, S.-C., Sun, T., Chan, H.S.O.: Chiral discrimination of enantiomers with a self-assembled monolayer of functionalized beta-cyclodextrins on Au surfaces. Tetrahedron Lett. **43**(15), 2863 (2002)

34. Rabe, J., Buttgenbach, S., Schroder, J., Hauptmann, P.: Monolithic miniaturized quartz microbalance array and its application

to chemical sensor systems for liquids. Sens. J. IEEE **3**(4), 361 (2003)

35. Ward, M.D., Buttry, D.A.: In situ interfacial mass detection with piezoelectric transducers. Science **249**(4972), 1000–1007 (1990)

36. Buttry, D.A., Ward, M.D.: Measurement of interfacial processes at electrode surfaces with the electrochemical quartz crystal microbalance. Chem. Rev. **92**(6), 1355–1379 (1992)

37. Mason, W.P.: Electromechanical Transducers and Wave Filters. D. Van Nostrand Co. (1948)

38. Martin, S.J., Granstaff, V.E., Frye, G.C.: Characterization of a quartz crystal microbalance with simultaneous mass and liquid loading. Anal. Chem. **63**(20), 2272–2281 (1991)

39. Lucklum, R., Hauptmann, P.: The Δf Δr QCM technique: an approach to an advanced sensor signal interpretation. Electrochim. Acta **45**(22–23), 3907–3916 (2000)

40. Lucklum, R., Behling, C., Hauptmann, P.: Gravimetric and non-gravimetric chemical quartz crystal resonators. Sens. Actuators B Chem. **65**(1–3), 277–283 (2000)

41. Lucklum, R., Behling, C., Hauptmann, P.: Role of mass accumulation and viscoelastic film properties for the response of acoustic-wave-based chemical sensors. Anal. Chem. **71**(13), 2488–2497 (1999)

42. Behling, C., Lucklum, R., Hauptmann, P.: Response of quartz-crystal resonators to gas and liquid analyte exposure. Sens. Actuators A Phys. **68**(1–3), 388–398 (1998)

43. Kanazawa, K.K., Gordon, J.G.: Frequency of a quartz microbalance in contact with liquid. Anal. Chem. **57**(8), 1770–1771 (1985)

44. Gadelle, A., DeFaye, J.: Selective halogenation at primary positions of cyclomaltooligosaccharides and a synthesis of per-3,6-anhydro cyclomaltooligosaccharides. Angew. Chem. Int. Ed. Engl. **30**(1), 78–80 (1991)

45. Rojas, M.T., Koniger, R., Stoddart, J.F., Kaifer, A.E.: Supported monolayers containing preformed binding-sites - synthesis and interfacial binding-properties of a thiolated beta-cyclodextrin derivative. J. Am. Chem. Soc. **117**(1), 336–343 (1995)

46. Berresheim, K., Mattern-Klosson, M., Wilmers, M.: A standard form of spectra for quantitative ESCA-analysis. Fresenius J. Anal. Chem. (Germany) **341**(1–2), 121–124 (1991)

47. Gonzalez-Gaitano, G., Rodrfguez, P., Isasi, J.R., Fuentes, M., Tardajos, G., Sanchez, M.: The aggregation of cyclodextrins as studied by photon correlation spectroscopy. J. Incl. Phenom. Macrocycl. Chem. **44**(1–4), 101–105 (2002)

48. D'Annibale, A., Regoli, R., Sangiorgio, P., Ferri, T.: Preparation and electrochemical characterization of a beta-cyclodextrin-based chemically modified electrode. Electroanalysis **11**(7), 505–510 (1999)

49. Liu, J., Alvarez, J., Ong, W., Roman, E., Kaifer, A.E.: Phase transfer of hydrophilic, cyclodextrin-modified gold nanoparticles to chloroform solutions. J. Am. Chem. Soc. **123**(45), 11148–11154 (2001)

50. Lee, J.-Y., Park, S.-M.: Electrochemistry of guest molecules in thiolated cyclodextrin self-assembled monolayers: An implication for size-selective sensors. J. Phys. Chem. B **102**(49), 9940–9945 (1990)

51. Moulder, J.F., Chastain, J.: Handbook of X-ray Photoelectron Spectroscopy: A Reference Book of Standard Spectra for Identification and Interpretation of XPS Data. Perkin-Elmer Corporation, Eden Prairie (1992)

52. Briggs, D., Beamson, G.: High Resolution XPS of Organic Polymers—The Scienta ESCA300 Database. Wiley Interscience (1992)

53. de Jong, M., Huskens, J., Reinhoudt, D.: Influencing the binding selectivity of self-assembled cyclodextrin monolayers on gold through their architecture. Chem. Eur. J. **7**(19), 4164–4170 (2001)

54. Brown, S.E., Easton, C.J., Kelly, J.B.: Surface plasmon resonance to determine apparent stability constants for the binding of cyclodextrins to small immobilized guests. J. Incl. Phenom. Macrocycl. Chem. **46**(3–4), 167–173 (2003)

55. David, C., Millot, M.C., Sebille, B.: High-performance liquid chromatographic study of the interactions between immobilized beta-cyclodextrin polymers and hydrophobically end-capped polyethylene glycols. J. Chromatogr. B Biomed. Sci. Appl. **753**(1), 93–99 (2001)

56. Karakasyan, C., Taverna, M., Millot, M.C.: Determination of binding constants of hydrophobically end-capped poly(ethylene glycols)s with beta-cyclodextrin by affinity capillary electrophoresis. J. Chromatogr. A **1032**(1–2), 159–164 (2004)

57. Wilchek, M., Bayer, E.A.: The avidin biotin complex in bioanalytical applications. Anal. Biochem. **171**(1), 1–32 (1988)

58. Krasilnikov, O.V., Sabirov, R.Z., Ternovsky, V.I., Merzliak, P.G., Muratkhodjaev, J.N.: A simple method for the determination of the pore radius of ion channels in planar lipid bilayer membranes. FEMS Microbiol. Immunol. **105**(1–3), 93–100 (1992)

59. Busse, S., DePaoli, M., Wenz, G., Mittler, S.: An integrated optical machzehnder interferometer functionalized by beta-cyclodextrin to monitor binding reactions. Sens. Actuators B Chem. **80**(2), 116–124 (2001)

60. Michalke, A., Janshoff, A., Steinem, C., Henke, C., Sieber, M., Galla, H.-J.: Quantification of the interaction between charged guest molecules and chemisorbed monothiolated beta-cyclodextrins. Anal. Chem. **71**(13), 2528–2533 (1999)

61. Hepel, M., Janusz, W.: Study of leuco-methylene blue film growth and its reoxidation on sulphur-modified Au-EQCN electrode. Electrochim. Acta **45**(22), 3785–3799 (2000)

62. Daikhin, L., Gileadi, E., Tsionsky, V., Urbakh, M., Zilberman, G.: Slippage at adsorbate-electrolyte interface. Response of electrochemical quartz crystal microbalance to adsorption. Electrochim. Acta **45**(22–23), 3615 (2000)

63. Tsionsky, V., Daikhin, L., Gileadi, E.: Response of the electrochemical quartz crystal microbalance for gold electrodes in the double-layer region. J. Electrochem. Soc. (USA) **143**(7), 2240–2245 (1996)

64. Tsionsky, V., Daikhin, L., Zilberman, G., Gileadi, E.: Response of the EQCM for electrostatic and specific adsorption on gold and silver electrodes. Faraday Discussions **107**, 337–350 (1997)

65. Tassew, N., Thompson, M.: RNA-peptide binding and the effect of inhibitor and RNA mutation studied by on-line acoustic wave sensor. Anal. Chem. 74(20):5313–5320 (2002)

66. Lyle, E.-L., Hayward, G.L., Thompson, M.: Acoustic coupling of transverse waves as a mechanism for the label-free detection of protein-small molecule interactions. Analyst **127**(12), 1596–1600 (2002)

67. McHale, G., Lucklum, R., Newton, M.I., Cowen, J.A.: Influence of viscoelasticity and interfacial slip on acoustic wave sensors. J. Appl. Phys. **88**(12), 7304–7312 (2000)

68. Ellis, J.S., Thompson, M.: Acoustic coupling at multiple interfaces and the liquid phase response of the thickness shear-mode acoustic wave sensor. Chem. Commun. **11**, 1310–1311 (2004)